A New Approach to Calculation of Three-Dimensional Flow in MHD Generators

Motoo Ishikawa* and Juro Umoto†
Kyoto University, Kyoto, Japan

A new scheme that treats three-dimensional phenomena in MHD generators is introduced. Parabolized Navier-Stokes equations are solved together with the κ-ϵ two-equation turbulence model and with the electrodynamic equations. The rational Runge-Kutta method is used along the main flow direction and the Galerkin finite element method in the perpendicular cross section. It is shown that, even when the MHD interaction is still low, three-dimensional effects become clear near open- and short-loading conditions in the case of a diagonal-type generator, since a relatively large J_x component is induced.

Nomenclature

B = z component of magnetic field
$b_{()}$ = const
$C_{()}$ = const
$c_{()}$ = const
E_x = x component of electric field
H = duct height in y direction
h = enthalpy
I = load current
$J_{()}$ = ( ) component of electric density
$\langle J_x \rangle$ = J_x averaged on y-z plane
L = duct length
m_0 = mass flow rate
p = local pressure
$\bar{p}$ = pressure averaged on y-z plane
q_w = heat flux on the duct wall
R = gas constant
S_{in} = inlet duct cross section
S_{out} = outlet duct cross section
T = gas temperature
u = x component of gas velocity
v = y component of gas velocity
W = duct height in z direction
w = z component of gas velocity
β = Hall parameter
Δx = mesh size along x direction
δ = boundary-layer thickness
ϵ = dissipation rate
θ = diagonal angle
κ = turbulent kinetic energy
μ_e = electrical mobility
μ_l = laminar viscosity
μ_t = turbulent viscosity
ρ = gas density
σ = gas conductivity
σ_h = Prandtl number for turbulent flow
σ_l = Prandtl number for laminar flow
σ_κ = Prandtl number for turbulence kinetic energy
σ_ϵ = Prandtl number for dissipation rate
Φ = electrical potential

Subscripts

c = values in the core flow
x = x component of parameter
y = y component of parameter
z = z component of parameter

Received Sept. 5, 1984; revision received May 31, 1985.

*Associate Professor, Department of Electrical Engineering.
†Professor, Department of Electrical Engineering.

I. Introduction

PHYSICAL processes in MHD generators are inherently three-dimensional, in both gasdynamics and electrodynamics, especially for large-scale, high-interaction machines. One of the most important phenomena is the secondary flow. Girshick and Kruger[1] reported an experimental evidence of the secondary flow induced in an MHD channel. A severe current concentration that occurred in a large MHD channel [the high-performance demonstration experiment (HPDE) at the Arnold Engineering Development Center (AEDC)[2]] seems to have been caused by the secondary flow. This effect of secondary flow had been predicted by Demetriades et al.[3]

Thus far, three groups have developed three-dimensional gasdynamical codes. A great deal of impressive work has been done by Demetriades et al.,[2-4] Vanka, Ahluwalia, and Doss,[5-7] and Liu et al.[8] All of these codes have proved to be powerful and useful. They were written with finite difference schemes. One of the present authors developed both an electrical three-dimensional code using a finite element method (FEM)[9,10] that can treat any configuration and gasdynamical two-dimensional codes.[9,11] In this paper, we extend our efforts and propose a new approach to solve gasdynamical three-dimensional phenomena in MHD channels using a FEM in the cross-sectional plane of an MHD generator. In principle, this code can analyze any shape of duct; however, only a rectangular duct will be discussed here.

Section II outlines a mathematical model in which parabolized three-dimensional gasdynamic and electrodynamical equations are described. Section III gives a brief description of the numerical scheme in which the rational Runge-Kutta (RRK) method is adopted together with the finite element method. Section IV shows the numerical results, where an intermediate-sized diagonal-type MHD generator is analyzed. Finally, Sec. V briefly summarizes the present proposal.

II. Mathematical Model

Gasdynamics Equations

The three-dimensional compressible turbulent flow inside an MHD channel is modeled in this section. The flow moves

predominantly along the axial direction (x direction), so that the parabolic approximation is adopted; i.e., diffusion terms in the axial direction are neglected and the pressure gradient in the axial momentum equation is considered to be uniform over the duct cross section. This simplification will not introduce significant errors when the flow is predominant along the axial direction and will save considerable computation time. Of course, this approach is not valid if shocks and/or boundary-layer separations occur.

The turbulence phenomena are described by a two-equation turbulence model in which two additional equations are solved, one for the turbulence kinetic energy κ and the other for the dissipation rate ϵ. The equations solved are as follows.

Mass continuity equation:

$$\frac{\partial(\rho u)}{\partial x}+\frac{\partial(\rho v)}{\partial y}+\frac{\partial(\rho w)}{\partial z}=0 \tag{1}$$

x momentum equation:

$$\rho u\frac{\partial u}{\partial x}+\rho v\frac{\partial u}{\partial y}+\rho w\frac{\partial u}{\partial z}+\frac{\partial \bar{p}}{\partial x}-\frac{\partial[(\mu_l+\mu_t)\partial u/\partial y]}{\partial y}$$
$$-\frac{\partial[(\mu_l+\mu_t)\partial u/\partial z]}{\partial z}-J_yB=0 \tag{2}$$

y momentum equation:

$$\rho u\frac{\partial v}{\partial x}+\rho v\frac{\partial v}{\partial y}+\rho w\frac{\partial v}{\partial z}+\frac{\partial p}{\partial y}-\frac{\partial[2(\mu_l+\mu_t)\partial v/\partial y]}{\partial y}$$
$$-\frac{\partial[(\mu_l+\mu_t)(\partial v/\partial z+\partial w/\partial y)]}{\partial z}+J_xB=0 \tag{3}$$

z momentum equation:

$$\rho u\frac{\partial w}{\partial x}+\rho v\frac{\partial w}{\partial y}+\rho w\frac{\partial w}{\partial z}+\frac{\partial p}{\partial z}$$
$$-\frac{\partial[(\mu_l+\mu_t)(\partial w/\partial y+\partial v/\partial z)]}{\partial y}-\frac{\partial[2(\mu_l+\mu_t)\partial w/\partial z]}{\partial z}=0 \tag{4}$$

Energy equation:

$$\rho u\frac{\partial h}{\partial x}+\rho v\frac{\partial h}{\partial y}+\rho w\frac{\partial h}{\partial z}-\frac{\partial[(\mu_l/\sigma_l+\mu_t/\sigma_h)\partial h/\partial y]}{\partial y}$$
$$-\frac{\partial[(\mu_l/\sigma_l+\mu_t/\sigma_h)\partial h/\partial z]}{\partial z}-u\frac{\partial \bar{p}}{\partial x}-v\frac{\partial p}{\partial y}-w\frac{\partial p}{\partial z}$$
$$-\frac{(J_x^2+J_y^2+J_z^2)}{\sigma}-(\mu_l+\mu_t)\left\{2\left[\left(\frac{\partial w}{\partial z}\right)^2+\left(\frac{\partial v}{\partial y}\right)^2\right]\right.$$
$$\left.+\left(\frac{\partial w}{\partial y}+\frac{\partial v}{\partial z}\right)^2+\left(\frac{\partial u}{\partial y}\right)^2+\left(\frac{\partial u}{\partial z}\right)^2\right\}=0 \tag{5}$$

Turbulence kinetic energy equation:

$$\rho u\frac{\partial \kappa}{\partial x}+\rho v\frac{\partial \kappa}{\partial y}+\rho w\frac{\partial \kappa}{\partial z}-\frac{\partial(\mu_t/\sigma_k\partial\kappa/\partial y)}{\partial y}$$
$$-\frac{\partial(\mu_t/\sigma_k\partial\kappa/\partial z)}{\partial z}-G+\rho\epsilon=0$$
$$G=\mu_t\left\{2\left[\left(\frac{\partial v}{\partial y}\right)^2+\left(\frac{\partial w}{\partial z}\right)^2\right]+\left(\frac{\partial u}{\partial y}\right)^2+\left(\frac{\partial u}{\partial z}\right)^2\right.$$
$$\left.+\left(\frac{\partial v}{\partial z}+\frac{\partial y}{\partial w}\right)^2\right\},\quad \sigma_k=1.0 \tag{6}$$

Turbulence dissipation rate equation:

$$\rho u\frac{\partial \epsilon}{\partial x}+\rho v\frac{\partial \epsilon}{\partial y}+\rho w\frac{\partial \epsilon}{\partial z}-\frac{\partial(\mu_t/\sigma_\epsilon\partial\epsilon/\partial y)}{\partial y}$$
$$-\frac{\partial(\mu_t/\sigma_\epsilon\partial\epsilon/\partial z)}{\partial z}-\frac{c_1G\epsilon}{\kappa}+\frac{c_2\rho\epsilon^2}{\kappa}=0 \tag{7}$$

where $\sigma_\epsilon=1.3$, $c_1=1.47$, and $c_2=1.92$.[6]

Turbulent viscosity:

$$\mu_t=c_D\rho\kappa^2/\epsilon,\quad c_D=0.09 \tag{8}$$

State equation:

$$p=\rho RT \tag{9}$$

In these equations, x is the coordinate along the channel axis; y the coordinate perpendicular both to channel axis and to magnetic field B; z the coordinate along the magnetic field; u, v, and w the x, y, and z components of the gas velocity, respectively; ρ the gas density; h the enthalpy; p the local pressure; $\bar{p}$ the average pressure on the y-z plane; R the gas constant; μ_l and μ_t the laminar and turbulent viscosity, respectively; σ_l, σ_h, σ_κ, and σ_ϵ the Prandtl numbers for the laminar flow, turbulent flow, turbulent kinetic energy, and dissipation rate, respectively; and J_x, J_y, and J_z the x, y, and z components of the electric current density, respectively; and σ the electrical conductivity of the working gas.

The mass continuity equation (1) is maintained indirectly in the following way. The gradient of average pressure $\bar{p}$ along the flow is determined to satisfy the overall mass continuity in the y-z plane,

$$m_0=\int\int\rho u\,dy\,dz \tag{10}$$

where m_0 is the mass flow rate. A few iterations are required to satisfy Eq. (10).

The local pressure is calculated by solving an elliptic equation derived by taking the divergence of the y and z momentum equations,[12]

$$\partial\left[\frac{\partial p}{\partial y}+J_xB+\frac{\partial(\rho uv)}{\partial x}+\frac{\partial(\rho vv)}{\partial y}+\frac{\partial(\rho wv)}{\partial z}\right]\Big/\partial y$$
$$+\partial\left[\frac{\partial p}{\partial z}+\frac{\partial(\rho uw)}{\partial x}+\frac{\partial(\rho vw)}{\partial y}+\frac{\partial(\rho ww)}{\partial z}\right]\Big/\partial z$$
$$+c_3\left[\frac{\partial(\rho u)}{\partial x}+\frac{\partial(\rho v)}{\partial y}+\frac{\partial(\rho w)}{\partial z}\right]=0 \tag{11}$$

where the third-order terms are neglected and c_3 is a constant. The last term is added to maintain the local mass continuity. The boundary condition for Eq. (11) is the usual Neumann condition.

The present model uses the "wall function" approach in order to treat near-wall regions.[6,13] This avoids using a very fine mesh in the regions close to walls.

Electrodynamical Equations

The basic equations are the Maxwell equations and the generalized Ohm's law. The magnetic Reynolds number is much smaller than unity, so that the applied magnetic field is given independently of the other quantities.

The infinite segmentation assumption reduces the basic three-dimensional equations to two-dimensional, thus alleviating numerical difficulties.[14] By introducing the elec-

trical potential Φ, the equation to be solved is derived as

$$\frac{\partial\{\sigma/(1+\beta^2)\,[\beta(E_x+vB)+(-\partial\phi/\partial y-uB)]\}}{\partial y} + \frac{\partial[\sigma(\partial\phi/\partial z)]}{\partial z} \tag{12}$$

where E_x is the x component of electric field and β the Hall parameter.

The magnitude of E_x is determined to satisfy the generator configuration (Faraday vs diagonal or mixed type) as well as the current leakage introduced in the x direction. The current leakage is calculated by a simplified model, i.e., a leakage resistance per unit length is given along the channel.

The boundary conditions for Φ are determined depending upon the channel configuration. For the Faraday channel, these are

$$J_z = 0 \quad \text{on insulating sidewalls}$$
$$\Phi = \text{const} \quad \text{on electrodes} \tag{13}$$

and for the diagonal (DCW) channel

$$\Phi = aE_x y \quad \text{on conducting sidewalls}$$
$$\Phi = \text{const} \quad \text{on electrodes} \tag{14}$$

where $a = \cot\theta$ and θ is the diagonal angle defined in Fig. 1.

III. Numerical Procedure

Equations (1-7) are parabolized so that a marching scheme is used in the flow direction—the rational Runge-Kutta (RRK) method,[15,16] which is unconditionally stable for a linear system in spite of being an explicit scheme.

For simplicity, let us consider

$$\frac{\partial U}{\partial x} = F \tag{15}$$

This method consists of two steps as follows:

First step (predictor)

$$g_1 = \Delta x F(U_n)$$
$$U_* = U_n + C_2 g_1 \tag{16}$$

where U_n is the solution at the nth node of the x direction, Δx the mesh size along the x direction, and C_2 a constant.

Second step (corrector)

$$g_2 = \Delta x F(U_*)$$
$$g_3 = b_1 g_1 + b_2 g_2$$
$$U_{n+1} = U_n + \frac{[g_1(g_1,g_3) - g_3(g_1,g_1)]}{(g_3,g_3)} \tag{17}$$

where b_1 and b_2 are constants and are selected as $C_2 = 0.5$, $b_1 = 2$, and $b_2 = -1$ in this paper.

In the y-z plane, Eqs. (2-7) are solved by the Galerkin finite element method (FEM) with the first-order triangle element.[9,10] In this connection, the usual FEM scheme requires a conversion of the matrix in each step along the x direction, resulting in a very long computation. To avoid this complexity, a concentration scheme of the FEM is adopted for the terms related to differential of x, leading the matrix to be diagonal. This scheme saves considerable computation time.

Equations (11) and (12) are solved by the usual Galerkin FEM as a boundary value problem.

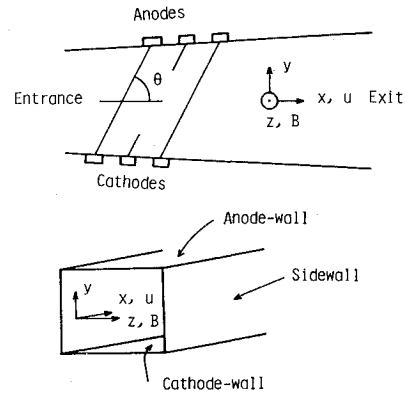

Fig. 1 Diagonal connecting wall of MHD channel.

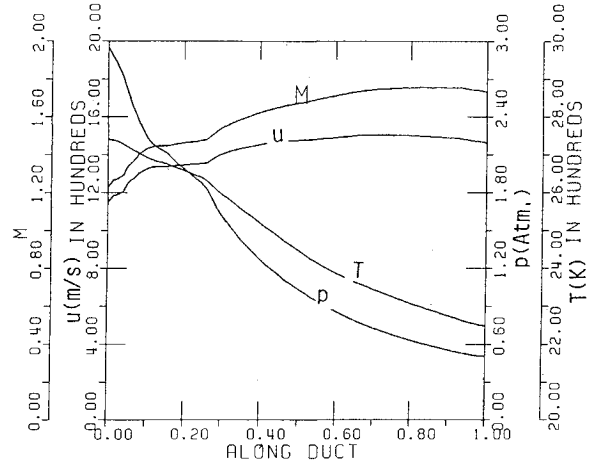

Fig. 2 Distribution of flow properties along channel without magnetic field (duct length 3m, all quantities are averaged on y-z plane in Figs. 2-4).

IV. Performance of a Diagonal-Type MHD Generator

Parameters of Channel

The MHD generator for which the numerical analysis will be carried out is the 45 deg diagonal conducting wall (DCW) channel designed for the Coal Fired Flow Facility (CFFF) at the University of Tennessee Space Institute (UTSI). This channel has a low mass flow (LMF) rate. Although no large three-dimensional effects are expected at the normal loading condition of this generator, relatively large three-dimensional effects are expected at off-nominal conditions. The reason is that the MHD interaction is rather low; however, a relatively large J_x component is generated at near open- and short-conditions due to the diagonal connection of electrodes. Figure 1 is a schematic diagram of the MHD channel analyzed in this paper.

The duct dimension and inlet conditions used are

$$L = 3\text{ m},\ S_{\text{in}} = 0.1016 \times 0.08255\text{ m}^2,\ S_{\text{out}} = 0.19243 \times 0.15824\text{ m}^2$$
$$u_c = 1200\text{ m/s},\ T_c = 2860\text{ K},\ p_c = 2.946\text{ atm},\ \delta = 0.01\text{ m} \tag{18}$$

where L is the duct length, S_{in} the inlet cross section, S_{out} the outlet cross section, subscript c the values in the core flow, and δ the boundary-layer thickness. It is assumed that the velocity and temperature profiles follow the one-seventh and one-fifth power laws, respectively, through the boundary layer in the inlet duct cross section. Other parameters are an equivalent wall roughness height of 2 mm, an electrical wall resistance of 10^4

Ω/m, and a wall temperature distributed linearly from 1850 K (inlet) to 1750 K (outlet). The power takeoff regions are treated in a simplified manner so that the load current is linearly distributed.

The thermodynamical properties of the working gas are given by

$$\sigma = 7.8272(T/2565)^{13.367}(p/1.175)^{-0.8930}\exp(8.9547 \times 10^{-3}T/2565), \text{ S/m}$$

$$\mu_e = 0.48(T/2565)^{0.9161}p^{-1.190}, 1/T$$

$$h = 1.4145\times 10^{6}p^{-0.0045923}(T\times 10^{-3})^{1.3423}, \text{ J/kg}$$

$$\rho = 0.39501p^{1.0016}(T\times 10^{-3})^{-1.1182}, \text{ kg/m}^3$$

$$\mu_l = 4.48699\times 10^{-5}(T\times 10^{-3})^{1.5}/(T\times 10^{-3}+0.1), \text{ kg/m s} \quad (19)$$

where μ_e is the electrical mobility. It should be noted that these evaluations do not necessarily coincide with the experimental or design conditions due to a lack of detailed data.

In the computations, the duct length is divided into 81 steps in the x direction, of which the total length is 3 m. The origin of x coordinate is the first power takeoff frame. In the y and z directions, 31 and 15 mesh points are used, respectively, while a half-region is treated in the z direction.

Non-MHD Case

Figure 2 shows the distributions of the velocity, Mach number, pressure, and temperature averaged on the y-z planes. Experimental results with similar inlet conditions have been given in Ref. 18, together with one-dimensional calculation results. Table 1 compares the three-dimensional calculation results with the data given in Ref. 18. The comparison indicates that

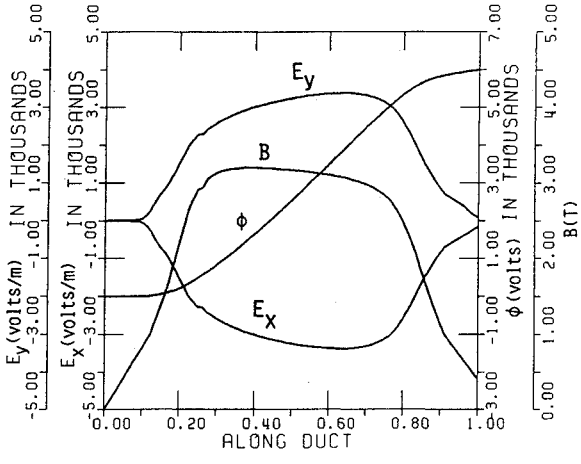

Fig. 3 Distribution of magnetic field and other electrical quantities for $I = 50$ A.

Table 1 Comparison of three-dimensional (3D) calculation results with experimental data

	3D (LMF1c-s data)	1D
Pressure (3 m), atm	0.492	0.5[a]
Heat flux, W/cm^2		
Entrance	337	280[a]
At 3 m	49.9	70[a]
Velocity (3 m), m/s	1553	1550[b]
Mach number (3 m)	1.836	1.85[b]
Temperature (3 m), K	2251	2300[b]

[a]Experimental data. [b]One-dimensional calculation results.

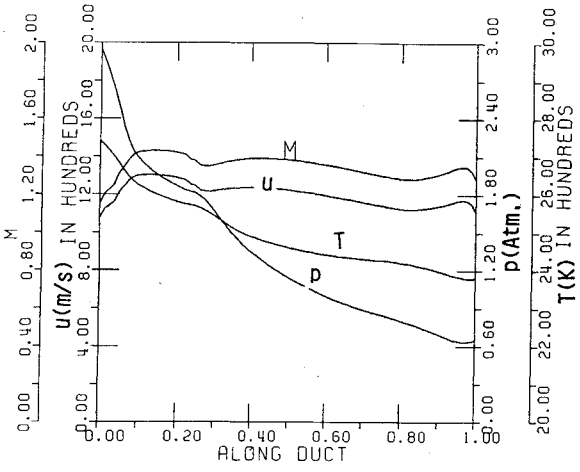

Fig. 4 Distribution of flow properties along channel for $I = 50$ A.

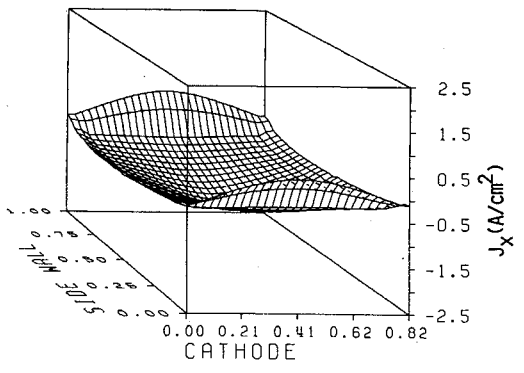

a) $I = 50$ A.

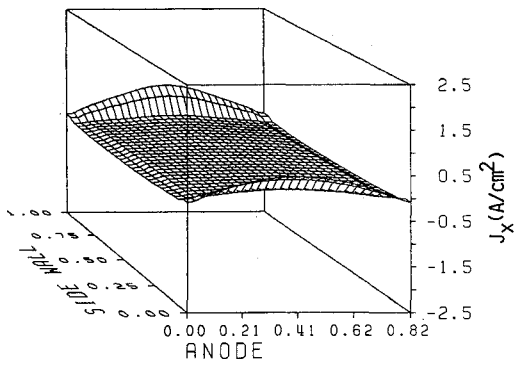

b) $I = 150$ A.

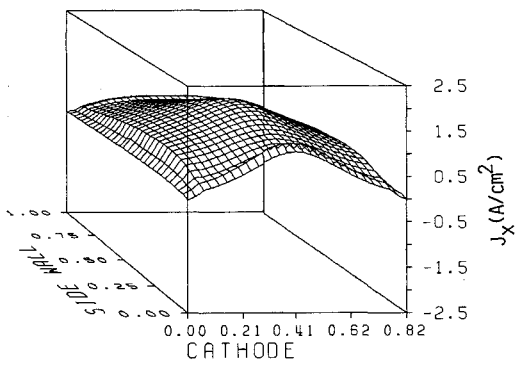

c) $I = 250$ A.

Fig. 5 Distribution of J_x in y-z plane ($x = 2.17$ m, duct size normalized by duct height H; $H = 0.170$ m and duct width $W = 0.139$ m).

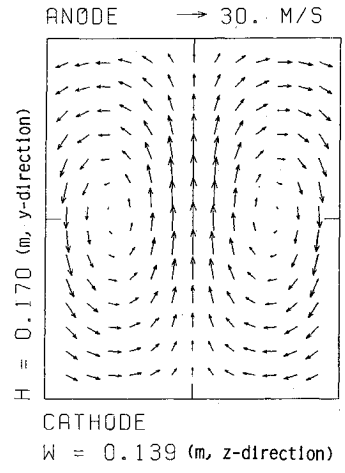

a) $I = 50$ A.

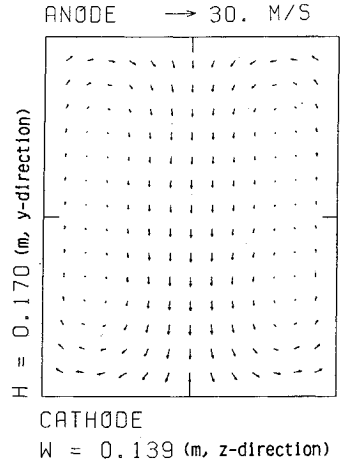

b) $I = 150$ A.

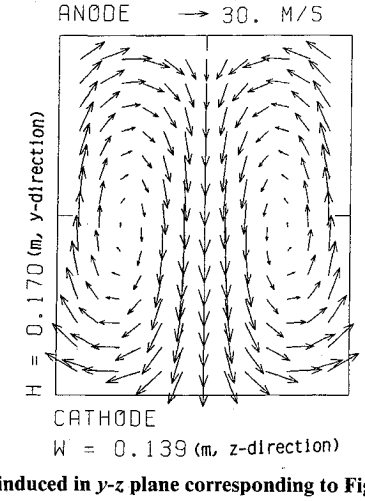

c) $I = 250$ A.

Fig. 6 Secondary flow induced in y-z plane corresponding to Figs. 5.

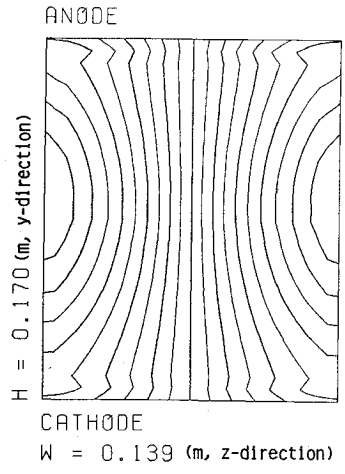

a) $I = 50$ A.

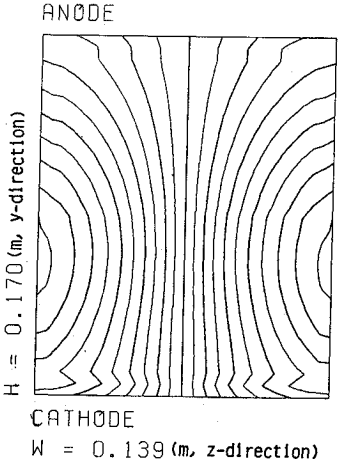

b) $I = 250$ A.

Fig. 7 Current distribution in y-z plane corresponding to Figs. 5 and 6.

the agreement in the pressure is good; however, some deviation is seen in the heat flux.

Secondary Flow in MHD Generator

Figure 3 shows the distribution of the magnetic field along the duct, together with distributions of the electric field and electrical potential for the case of load current $I = 50$ A. Figure 4 shows the distribution of the flow parameters averaged in the y-z plane. Near the entrance, the flow is accelerated in the way similar to the non-MHD case (see Fig. 2) and then the Lorentz force decelerates the flow slightly when it begins to diffuse near the exit.

With these conditions, the short-circuit current is about 295 A, the open-circuit voltage is about 7.30 kV, and the maximum output power is about 535 kW. These values agree roughly with the results obtained by a two-dimensional analysis,[17] such that the three-dimensional effects have no large influence on the overall performance of the present generator.

However, the interaction between the gasdynamics and electromagnetic effects results in a three-dimensional phenomenon; a secondary flow and then a significant asymmetry between the anode and cathode, especially at off-nominal loading conditions. In this connection, the pressure-based interaction parameter is about 0.5 and the isentropic efficiency about 0.4, depending upon the loading conditions.

Figure 5 shows the distributions of J_x on the y-z plane at $x = 2.17$ m for $I = 50$, 150, and 250 A, respectively. Figure 5a corresponds to the near-open-circuit condition so that the value of J_x is negative except near those electrode regions in which the cold boundary layer induces a positive J_x. Figure 5b corresponds to the near-nominal condition, resulting in very small J_x except in the near-electrode regions. Figure 5c shows the large J_x for the near-open-circuit condition. Figure 6 illustrates the secondary flow on the same plane. In the case of $I = 50$ A, the flow is generated toward the anode due to the negative J_x shown in Fig. 5a, whereas it is directed toward the cathode in the case of $I = 250$ A due to the positive J_x (see Fig. 5c). In the case of $I = 150$ A, which is almost at the nominal condition, the secondary flow is very weak and is directed toward the cathode in spite of the negative value of $\langle J_x \rangle$. This is because a large positive J_x is induced adjacent to the anode

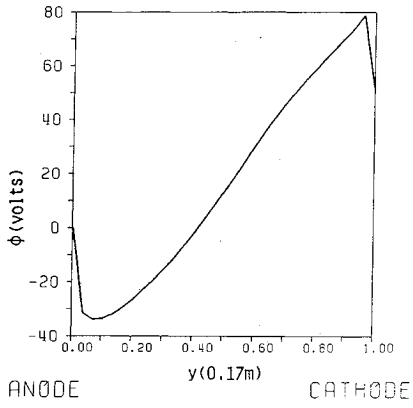

Fig. 8 Potential distribution along y direction at center of z direction for $I=250$ A ($x=2.17$ m).

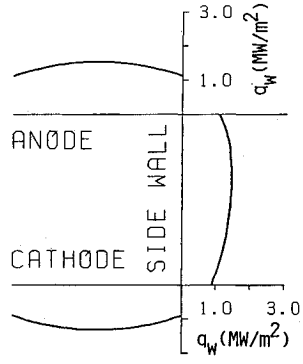

a) $I=50$ A.

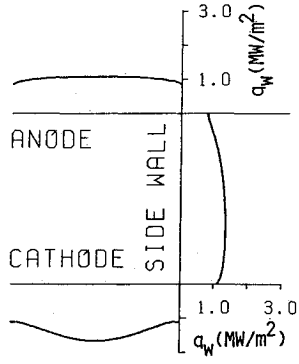

b) $I=250$ A.

Fig. 9 Heat flux along duct wall corresponding to Figs. 5-7 ($x=2.17$ m).

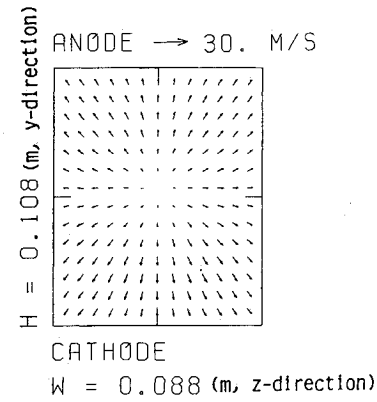

a) $x=0.37$ m.

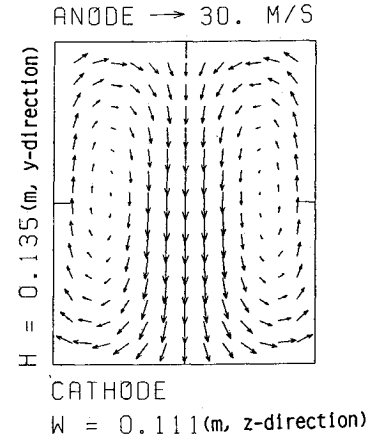

b) $x=1.27$ m.

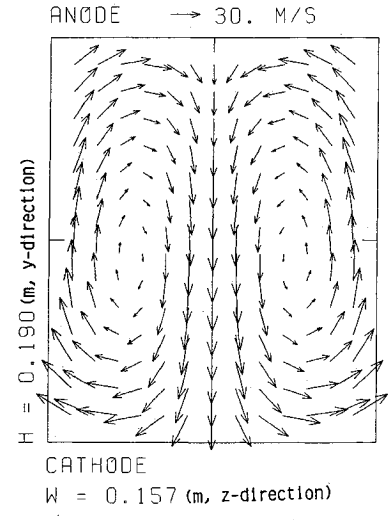

c) $x=2.71$ m.

Fig. 10 Development of secondary flow along channel $I=250$ A.

and cathode, shown in Fig. 5b, leading to an acceleration toward the cathode there; this generator is rather small, so that the phenomena near boundary layer become dominate.

Figure 7 shows the current distribution in the same plane for $I=50$ A and 250 A. In the case of $I=50$ A, a slight current concentration is seen at the center of anode, whereas the current concentrates at the center of cathode for $I=250$ A. Figure 8 shows an asymmetry of the potential distribution between the anode and cathode in the case of $I=250$ A. The electrode voltage drop at the anode is about 55 V, whereas the electrode voltage drop at the cathode is about 40 V with a total voltage drop of 95 V. The electrode voltage drop at the anode is about 1.4 times as large as that at the cathode. The difference is induced by the secondary flow. Figure 9 shows the distribution of heat flux q_w along the duct wall for $I=50$ and 250 A. The heat flux is larger at the anode side than at the cathode side in the case of $I=50$ A, whereas a contrary result is seen for $I=250$ A. These phenomena are also caused by the secondary flow.

Similar calculation results were reported in Ref. 7, where near the short-circuit condition the secondary flow was induced to the cathode at the core region, whereas the secondary flow was directed to the anode in the case of the open-circuit condition. These results were obtained for a large channel, while the present paper shows that similar three-dimensional phenomena can be induced and observed in a rather small channel. The present calculation also shows that there is a possibility that a cathode concentration can be induced in a small channel, as reported in Reference 19.

V. Conclusions

A new scheme is introduced that treats three-dimensional phenomena in MHD generators, one of which is the develop-

ment of a secondary flow perpendicular to the main flow.

Even when the MHD interaction is still low, the three-dimensional effect becomes inportant near open- and short-loading conditions in the case of diagonal-type generators, since a relatively large J_x component is produced under these conditions. The asymmetry, both in the gasdynamic and electrodynamic fields, will be induced and observed between the anode and cathode in a rather small diagonal channel.

Acknowledgment

This study was supported in part by a Scientific Research Fund from the Ministry of Education, Japan, Contract 58045090. The computations were done on the FACOM M382 at the Data Processing Center, Kyoto University.

References

[1]Girshick, S. L. and Kruger, C. H., "Evidence of Secondary Flow in Faraday MHD Generators," *Proceedings of 21st Symposium on Engineering Aspects of MHD,* Argonne, IL, June 1983, pp. 3.5.1-3.5.11.

[2]Demetriades, S. T., Maxwell, C.D., and Oliver, D.A., "Progress in Analytical Modeling of MHD Generators, II," *Proceedings of 21st Symposium on Engineering Aspects of MHD,* Argonne, IL, June 1983, pp. 3.1.1-3.1.20.

[3]Demetriades, S. T., Oliver, D. A., Swean, T.F., and Maxwell, C. D., "On the Magnetoaerothermal Instability," AIAA paper 81-0248, Jan. 1981.

[4]Demetriades, S. T., Argyropoulos, G. S., and Maxwell, C. D., "Progress in Analytical Modeling of MHD Power Generators," *Proceedings of 12th Symposium on Engineering Aspects of MHD,* Argonne, IL, March 1972, pp. I.5.1-I.5.13.

[5]Vanka, S. P. and Ahluwalia, R. K., "Three-Dimensional Flow and Heat Transfer Development in MHD Channels," AIAA Paper 81-0247, Jan. 1981.

[6]Vanka, S. P., Anluwalia, R. K., and Doss, E. D., "Three-Dimensional Analysis of MHD Generators and Diffusers," Argonne National Laboratory Argonne, IL, Rept. ANL/MHD-82-4, 1982.

[7]Doss, E. D. and Ahluwalia, R. K., "Three-Dimensional Flow Development in MHD Generators at Part Load," AIAA Paper 82-0324, Jan. 1982.

[8]Liu, B. L., Schmidt, H., and Wu, Y. C. L., "Simplified Three Dimensional Fluid and Electrodynamic Calculations For an MHD Loading Analysis," AIAA Paper 82-0921, Jan. 1982.

[9]Ishikawa, M., "Coupled Effects of Electrodynamics and Gasdynamics in Disk Type MHD Generator," *Proceedings 7th International Conference on MHD Power Generation*, Moscow, U.S.S.R., June 1980, pp. 503-509.

[10]Ishikawa, M. and Wu, Y. C. L., "Three-Dimensional Current Distribution and Slagging Effects in Coal Fired MHD Channel," *Proceedings 19th Symposium on Engineering Aspects of MHD*, Tullahoma, TN, June 1981, pp. 5.2.1-5.2.7.

[11]Ishikawa, M., Liao, Y. F., Wu, Y. C. L., and Scott, M. H., "Time-Dependent Analysis of Fault Currents in Mid-Channel Power Takeoff of a DCW MHD Generator," *Proceedings 20th Symposium on Engineering Aspects of MHD*, Irvine, CA, June 1982, pp. 7.3.1-7.3.7.

[12]Roberts, D. W. and Forester, C. K., "Parabolic Procedure for Flows in Ducts with Arbitrary Cross Section," *AIAA Journal*, Vol. 17, Jan. 1979, pp. 33-40.

[13]Launder, B. E. and Spalding, D. B., "The Numerical Computation of Turbulent Flows," *Computer Methods in Applied Mechanics and Engineering*, Vol. 3, 1974, pp. 269-289.

[14]Ishikawa, M. and Umoto, J., "Effects of Internal and External Connection of Electrodes in Diagonal Type Nonequilibrium Plasma MHD Generator," *Journal of Nuclear Science and Technology*, Vol. 15, No. 2, 1978, pp. 91-99.

[15]Haier, E., "Unconditionally Stable Explicit Methods for Parabolic Equations," *Numerische Mathematik*, Vol. 35, 1980, pp. 52-68.

[16]Satofuka, N., "Modified Differential Quadrature Method for Numerical Solution of Multi-Dimensional Flow Problems," *Proceedings International Symposium Applied Mathematics and Information Science,* Kyoto, Japan, March 1982, pp. 5.7-5.14.

[17]Lineberry, J. T., Galanga, F. L., Clemons, R. W., and Wu, Y. C. L., "Performance Predictions for the CFFF Low Mass Fow MHD Generator," *Proceedings Specialists Meeting on Coal Fired MHD Power Generation,* Sydney, Australia, Nov. 1981, pp. 6.5.1-6.5.5.

[18]Lineberry, J. T., Galanga, F. L. and Gonzalez, D. E., "Gas Dynamic and Heat Transfer Evaluation of the CFFF LMF1 Flow Train," *Proceedings 21st Symposium on Engineering Aspects of MHD,* Argonne, IL, June 1983, pp. 2.5.1-2.5.18.

[19]Hruby, V. J. et al., "AERL MHD Program Overview," *Proceedings Second Workshop of Japan-U.S. Cooperative Program,* Vol. I, Butte, MT, Oct. 1984, pp. 1-11.